https://doi.org/10.21122/1029-7448-2023-66-3-205-214

UDC 62-83-52(075.8)

Reference Input Signals Formation for Induction Motor Control in Traction Drive

O. F. Opeiko[1)]

[1)]Belarusian National Technical University (Minsk, Republic of Belarus)

Abstract. The purpose of this work is to build the analytical improved (with resistances estimation) real time computation of the reference inputs for rotor flux and torque in the vector control system of an induction motor of a traction electric drive. The reference inputs must maximize electromagnetic torque in conditions of voltage source instability, particularly in magnetic field weakening mode. The conventional way to control the field weakening mode is to form flux coupling task inversely proportional to the speed or inversely proportional to the square of the speed in second and third zones respectively. Such reference input signals are not able to provide the maximum torque capability over the entire speed range, and the improved torque capability is achieved in different ways. For instance, voltage feedback is useful for the torque capability enhancement in conditions of internal and external perturbations. A wide change in speed with the weakening of the flux reveals the nonlinear properties of an induction electric motor. However, in vector control systems, proportional-integrating (PI) regulators are usually used. Therefore, firstly, linear PI controllers must be robust, and secondly, the reference input signals for flux and torque must guaranty linear, not saturated state of each PI controller. The proposed expressions for calculating reference inputs for induction motor rotor flux and electromagnetic torque as functions of actual rotor speed are the approximate expressions. The estimation of the possible error shows that the error is acceptable. Simulation is performed for the vector control system of an induction motor and taking into account the calculation of the control signal by the microcontroller and the dynamics of the frequency invertor. The simulation of the resulting system validates the effectiveness of the control system using the proposed expressions for the formation of real-time reference input signals for setting the flux and torque.

Keywords: vector control, reference input signals, induction motor, electromagnetic torque, field weakening, simulation

For citation: Opeiko O. F. (2023) Reference Input Signals Formation for Induction Motor Control in Traction Drive. *Energetika. Proc. CIS Higher Educ. Inst. and Power Eng. Assoc.* 66 (3), 205–214. https://doi.org/10.21122/1029-7448-2023-66-3-205-214

Формирование сигналов задания системы тягового асинхронного электропривода

О. Ф. Опейко[1)]

[1)]Белорусский национальный технический университет (Минск, Республика Беларусь)

Реферат. Цель данной работы – формирование в реальном времени сигналов задания потокосцепления и момента в системе векторного управления асинхронным электродвигателем

Адрес для переписки	**Address for correspondence**
Опейко Ольга Федоровна	Opeiko Olga F.
Белорусский национальный технический университет	Belarusian National Technical University
просп. Независимости, 65,	65, Nezavisimosty Ave.,
220013, г. Минск, Республика Беларусь	220013, Minsk, Republic of Belarus
Тел.: +375 17 293-95-61	Tel.: +375 17 293-95-61
oopeiko@bntu.by	oopeiko@bntu.by

тягового электропривода. Сигналы задания должны максимизировать момент в условиях нестабильности напряжения источника питания, в частности в режиме ослабления магнитного поля. Обычный способ управления режимом ослабления поля заключается в формировании задания потокосцепления обратно пропорционально скорости либо квадрату скорости. Так формируемые сигналы задания не способны обеспечить максимум располагаемого момента во всем диапазоне изменения скорости, и увеличение располагаемого момента достигается различными путями. Например, обратная связь по напряжению используется для увеличения располагаемого момента в условиях внутренних и внешних возмущений. Широкое изменение скорости при ослаблении потокосцепления выявляет нелинейные свойства асинхронного электродвигателя. Однако в системах векторного управления обычно применяются пропорционально-интегрирующие (ПИ) регуляторы. Следовательно, во-первых, линейные ПИ-регуляторы должны быть робастными, во-вторых, сигналы задания для потокосцепления и момента должны гарантировать линейное без насыщения функционирование каждого ПИ-регулятора системы управления. Предложенные выражения для расчета входных сигналов задания для потокосцепления ротора и электромагнитного момента как функции текущего значения скорости ротора являются приближенными выражениями. Оценка возможной погрешности показывает, что погрешность допустима. Имитационное моделирование выполнено для системы векторного управления асинхронным электродвигателем и с учетом вычисления сигнала управления микроконтроллером и динамики преобразователя частоты. Имитационное моделирование системы подтверждает эффективность управления с применением предложенных выражений для формирования в реальном времени сигналов задания потокосцепления и момента.

Ключевые слова: векторное управление, ориентированное по потокосцеплению ротора, сигналы задания, асинхронный электродвигатель, электромагнитный момент, ослабление поля, имитационное моделирование

Для цитирования: Опейко, О. Ф. Формирование сигналов задания системы тягового асинхронного электропривода / О. Ф. Опейко // *Энергетика. Изв. высш. учеб. заведений и энерг. объединений СНГ*. 2023. Т. 66, № 3. С. 205–214. https://doi.org/10.21122/1029-7448-2023-66-3-205-214

Introduction

The control of induction motor in the field weakening region became an actual problem with the vector control development [1–8]. The early implementations of the flux weakening control of rotor or stator field-oriented control and direct torque control use the simple inverse of the rotor speed method. As it was shown in [5] and [6], such a control cannot maintain maximum torque capability over the entire speed range. The improved torque capability is achieved when the stator flux reference is varied as the inverse of the rotor speed [5–8]. As usual, the torque is maximized with omission of the stator resistance [5, 8]. The inverter voltage limit and current limit are considered simultaneously in the (d, q)-axis plane of the stator current to obtain an optimal rotor flux command [6]. Three sub regions of the speed can be recognised [5, 6].

The papers [7–24] present ways to improve the torque maximization when the field is weakening. Closed-loop methods use the proportional integral (PI) controllers to adjust the flux level when the voltage commands from current regulators are beyond the inverter voltage limit [15, 16]. The advantage of the closed loop methods is the relative independence of machine parameters. However, the additional PI controllers make the controller more complicated and tuning more difficult. In [8, 11] the control schemes are presented and analysed

for the field-weakening region. These control schemes fully utilize the maximum available voltage and current and can produce the maximum possible torque in the entire field-weakening region. The field weakening is mainly actual for the traction drives and others wide speed range applications. For a traction drive, especially for the electric vehicles, efficiency of induction motors applications depends hardly on the field weakening control [14, 15, 25–28]. So, in the papers [5–24, 29] the field weakening control synthesis comprises two directions. Firstly, the reference values are designed [5, 6, 29]. Next, the feedback control is developed for the robustness improvement. Mainly, for torque maximisation, the voltage loop is in usage [7–22]. In [29] the artificial neural network is applied for flux and speed control. As it was shown in [14, 15] when extracting the possible output torque for deep flux-weakening operation, the torque ripples are typical. The band-stop filter is proposed in [14], but that means the stability margin reducing, and also the system becomes more complicate. Hence, the reason is to provide near maximum torque control avoiding torque ripples.

As usual, in vector control for induction motors PI controllers are in employment. That means the hidden assumption of plant linearity or linearization. However, in field weakening region the induction motor nonlinearity is revealing. But the linear control still effective, when the reference values are correctly constructed, such all regulators still not saturated.

In this work, the aim is to build the analytical improved (with resistances estimation) real time computation of the references for rotor flux and torque in field weakening region to maximise torque value for induction motor in the vector control traction drive system. The reference inputs must maximize electromagnetic torque in conditions of voltage source instability, particularly in field weakening region. The electromagnetic parameters of induction motor are assumed to be known from the on line identification [30–32].

Induction motor control in the traction drive

In the traction drive, the flux and torque control are useful. The input u_C of references block determines acceleration or deceleration of traction motor. The car driver's command u_C must provide the reference rotor flux Ψ^* and current i_q^* computation, as shown in the control system block diagram (Fig. 1).

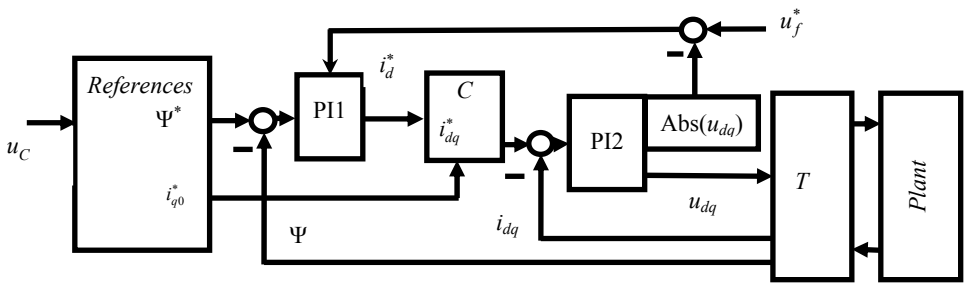

Fig. 1. The induction motor control system

That denotes the torque reference as $M^* = k_M \Psi^* i_q^*$, but instead of M^* the current component i_q^* is in employment as a reference for current control. The control structure uses plants variables in the synchronous frame (*d*, *q*). The PI1 is the flux controller, its output i_d^* is the magnetizing current reference value. Block *C* corrects current reference value i_{q0}^* depending on i_d^* through the conditions for the magnitude of the stator current vector: if $i_d^{*2} + i_{q0}^{*2} < I_m^2$, then $i_q^* = i_{q0}^*$, otherwise $i_q^* = \left(I_m^2 - i_d^{*2}\right)^{1/2}$. The flux PI controller PI1 has two inputs to estimate the voltage source u_f^* [7–16] and flux Ψ^* reference values. The magnitude $u_f = Abs\left(u_{dq}\right) = \left(u_d^2 + u_q^2\right)^{1/2}$ is needed for the comparisons with source voltage u_f^*. The block *T* offers coordinate and phase direct and inverse transforms, and the block *Plant* contains the induction motor with frequency inverter as voltage source.

In the synchronous frame (*d, q*) the induction motor dynamics can be described with state vector $x^T = \left(\Psi_d, i_d, i_q\right)$ and control vector $u_{dq}^T = \left(u_d, u_q\right)$, where $\Psi = \left(\Psi_d, \Psi_q\right)$ is the rotor flux vector with $\Psi_d = 0$, and $i_{dq}^T = \left(i_d, i_q\right)$ is the stator current vector. The equations are as follow:

$$\begin{aligned}
\dot{\Psi}_d &= -\alpha\Psi_d + \alpha L_{12} i_d; \\
\frac{di_d}{dt} &= \left(-R_e i_d + u_d + k_2 \alpha \Psi_d\right) L_e^{-1} + \omega_0 i_q; \\
\frac{di_q}{dt} &= \left(-R_e i_q + u_q - k_2 p_p \bar{\omega} \Psi_d\right) L_e^{-1} - \omega_0 i_d;
\end{aligned} \tag{1}$$

$$J\dot{\omega} = M - M_C; M = k_M \Psi_d i_q. \tag{2}$$

In these expressions the stator and rotor resistances R_1, R_2, Ω; the stator and rotor inductances L_1, L_2, *H* and the mutual inductance L_{12}, *H* are employed as follow: $\alpha = R_2 / L_2$, $k_1 = L_{12} / L_1$, $k_2 = L_{12} / L_2$, $R_e = R_1 + k_2^2 R_2$. Then, the leakage factor is $\sigma = 1 - k_1 k_2$, and the inductance $L_e = \sigma L_1$ characterizes the flux leakage. The rotor angular speed is ω, rad/s, and $\bar{\omega} = \omega p_p$, where p_p is the pair of pole number. The expression (2) for electromagnetic torque *M* contains the coefficient $k_M = (3/2) k_2 p_p$, *J* is the moment of inertia, and M_C is the load torque. It is assumed, that parameters L_{12}, R_1, L_1, $T_2 = L_2 / R_2$ are online identified [30–32].

Maximum torque conditions

The reference values for flux and current components for torque maximization must be evaluated for the steady state conditions in (*d*, *q*) frame. The steady state equations are produced from (1), (2) as follow:

$$
\begin{aligned}
0 &= -\alpha\Psi_d + \alpha L_{12} i_d;\\
0 &= \left(-R_e i_d + u_d + k_2 \alpha \Psi_d\right) L_e^{-1} + \omega_0 i_q;\\
0 &= \left(-R_e i_q + u_q - k_2 p_p \overline{\omega} \Psi_d\right) L_e^{-1} - \omega_0 i_d;
\end{aligned} \tag{3}
$$

$$
M = M_C;\ M = k_M \Psi i_q;\ \omega_s = \omega_0 - \overline{\omega} = \alpha i_q / i_d\,. \tag{4}
$$

The first harmonic magnitudes U, I of voltage and current are defined from the expressions $U^2 = u_d^2 + u_q^2$, $I^2 = i_d^2 + i_q^2$. From (3) and with respect to the expression $\omega_s = \alpha\, i_q/i_d$ for the slip frequency in the steady state, the current can be expressed as $I^2 = i_d^2\left(1 + \omega_s^2/\alpha^2\right)$. So, the stator voltage magnitude is $U^2 = i_d^2 f\left(\omega_s, \omega_0\right)$. With $\alpha_1 = R_1/L_1$, $\alpha_1 = R_1/L_1$, the function $f\left(\omega_s, \omega_0\right)$ can be written in form $f\left(\omega_s, \omega_0\right) = 2L_1^2\left(\left(1 + \omega_s^2/\alpha^2\right)\left(\sigma^2\omega_0^2 + \alpha_1^2\right) + \omega_0^2 - \sigma^2\omega_0^2 + 2\left(1-\sigma\right)\alpha_1\omega_s\,\omega_0/\alpha\right)$, or as follow:

$$
f\left(\omega_s, \omega_0\right) = 2L_1^2\left(A_2\omega_s^2 + A_1\omega_s + A_0\right). \tag{5}
$$

The rotor flux angular speed ω_0 is unmeasured and can be calculated from the rotor speed $\overline{\omega}$, as follow: $\omega_0 = \omega_s + \overline{\omega}$. The variables A_i (i = 0, 1, 2) depend on electromagnetic parameters and ω_0 as follow: $A_2 = \left(\alpha_1^2 + \sigma^2\omega_0^2\right)\alpha^{-2}$, $A_1 = 2\omega_0\alpha_1\alpha^{-1} \times$ $\times\left(1-\sigma\right)$, $A_0 = \omega_0^2 + \alpha_1^2$. The torque (4), in the form $M = k_M L_{12} i_d^2 \omega_s/\alpha$ permits to express the condition $\partial M/\partial\omega_s = k_M L_{12}\left(i_d^2 + 2i_d\partial i_d/\partial\omega_s\right)/\alpha = 0$ of torque maximum, depending on sliding frequency ω_s, in the form $i_d^2 + \partial\left(i_d^2\right)/\partial\omega_s = 0$. But the torque maximization must be done with voltage restriction $U^2 = i_d^2 f\left(\omega_s\omega_0\right)$, where $\partial U^2/\partial\omega_s = 0$. The nonlinear algebraic equations can be represented as follow:

$$
i_d^2 + \partial\left(i_d^2\right)/\partial\omega_s = 0;
$$

$$
\frac{\partial\left(i_d^2\right)}{\partial\omega_s} f\left(\omega_s, \omega_0\right) + i_d^2 \frac{\partial f\left(\omega_s, \omega_0\right)}{\partial\omega_s} = 0;\ \omega_s = \omega_0 - \overline{\omega} = \alpha i_q / i_d\,. \tag{6}
$$

The function f derivative is $\partial f\left(\omega_s, \omega_0\right)/\partial\omega_s = L_1^2\left(2A_2\omega_s + A_1\right)$. We must submit $\partial\left(i_d^2\right)/\partial\omega_s = -i_d^2$ from the first equation (6) to the second one with respect to (5) and then divide by $L_1{}^2\, i_d^2 > 0$. Hence, for the maximizing sliding frequency ω_s^*, we have the equation $-\left(A_2\omega_s^{*2} + A_1\omega_s^* + A_0\right) + \omega_s^*\left(2A_2\omega_s^* + A_1\right) = 0$. It is equal to $A_2\omega_s^{*2} - A_0 = 0$. So, the optimal value ω_s^* as a function of the synchronous frequency ω_0 becomes as follow:

$$\omega_s^{*2} = \alpha^2 \frac{\left(\alpha_1^2 + \omega_0^2\right)}{\left(\alpha_1^2 + \sigma^2\omega_0^2\right)}. \tag{7}$$

As a result, the function $f\left(\omega_s^*, \omega_0\right) = f^*\left(\omega_0\right)$ takes a form

$$f^*\left(\omega_0\right) = L_1^2\left(\alpha_1^2 + \omega_0^2 + \alpha_1\omega_0\left(1-\sigma\right)\sqrt{\left(\alpha_1^2 + \omega_0^2\right)\Big/\left(\alpha_1^2 + \sigma^2\omega_0^2\right)}\right)2. \tag{8}$$

With respect to the expression (5) $\omega_s = \alpha\ i_q/i_d$ the optimal references for $\Psi = L_{12}i_d$ and i_q^* take a form

$$\Psi_d^* = \frac{L_{12}U}{\sqrt{f^*\left(\omega_0\right)}};\ i_q^* = \frac{\omega_s^*}{\alpha}i_d^* = \frac{\omega_s^*}{\alpha}\frac{U}{\sqrt{f^*\left(\omega_0\right)}}. \tag{9}$$

The expressions (7)–(9) contain the variable ω_0, which is not measurable. The rotor speed ω is measured by sensor or estimated. In case of submitting the value of $\overline{\omega} = \omega p_\Pi$ instead of ω_0, the error occurs. The absolute error may be evaluated from (7) with respect to $\Delta\left(\omega_s^{*2}\right) = 2\omega_s^*\Delta\omega_s^*;\ \ \Delta\left(\omega_0^2\right) = 2\omega_0\Delta\omega_0$, and takes a form

$$\Delta\omega_s^* = \sqrt{\frac{d\left(\omega_s^{*2}\right)}{d\left(\omega_0^2\right)}\Delta\left(\omega_0^2\right)} = \frac{\alpha^2\alpha_1^2\left(1-\sigma^2\right)}{\left(\alpha_1^2 + \sigma^2\omega_0^2\right)^2}\frac{\omega_0}{\omega_s^*}\Delta\omega_0. \tag{10}$$

The relative error $\delta_s = \Delta\omega_s^*/\omega_s^*$ depending on $\delta_0 = \Delta\omega_0/\omega_0$ derives from (10) and (7) and takes a form

$$\delta_s = \frac{\left(1-\sigma^2\right)}{\left(1 + \sigma^2\omega_0^2/\alpha_1^2\right)\left(\alpha_1^2/\omega_0^2 + 1\right)}\delta_0. \tag{11}$$

The denominator has a minimum on $\omega_0^2 = \alpha_1^2/\sigma$, so, the maximal error is $\delta_{s\max} = \delta_0\left(1-\sigma^2\right)\Big/\left(1+\sigma\right)^2$. However, in field weakening region, as usual, $\omega_0^2 > \alpha_1^2/\sigma^2$, then $\delta_s \le 0.5\delta_0\left(1-\sigma^2\right)\Big/\left(1+\sigma^2\right)$. If in expressions (7)–(9) the value ω_0 is changed by $\overline{\omega} = \omega_0 - \omega_s$, the error $\Delta\omega_0 = \omega_s$ and relative error $\delta_0 = \Delta\omega_0 = \omega_s/\omega_0$ occur in slip frequency ω_s computation. But the slip frequency in (8) is growing with frequency ω_0, and its limit is $\omega_s^* = \alpha/\sigma$. Consequently, the relative error for $\overline{\omega} = \omega_0 - \omega_s$ is as follow:

$$\delta_s \le \frac{\left(1-\sigma^2\right)}{2\left(1+\sigma^2\right)}\frac{\alpha}{\sigma\omega_0}. \tag{12}$$

Hence, with small σ, the relative error of calculating ω_s^* is lower, then a half of the motor slip $s = \omega_s^* / \omega_0 = \alpha / \omega_0 \sigma$. This is acceptable, and expressions (7)–(9) after changing $\bar{\omega} = \omega_0 - \omega_s$ instead of ω_0 takes a form:

$$\omega_s^{*2} = \alpha^2 \frac{\left(\alpha_1^2 + \bar{\omega}^2\right)}{\left(\alpha_1^2 + \sigma^2 \bar{\omega}^2\right)};$$

$$f^*\left(\bar{\omega}\right) = L_1^2 \left(\alpha_1^2 + \bar{\omega}^2 + \alpha_1 \bar{\omega}\left(1 - \sigma\right) + \sqrt{\left(\alpha_1^2 + \bar{\omega}^2\right) / \left(\alpha_1^2 + \sigma^2 \bar{\omega}^2\right)}\right); \qquad (13)$$

$$\Psi_d^* = \frac{L_{12} U}{\sqrt{f^*\left(\bar{\omega}\right)}}; \quad i_q^* = \frac{\omega_s^*}{\alpha} i_d^* = \frac{\omega_s^*}{\alpha} \frac{U}{\sqrt{f^*\left(\bar{\omega}\right)}}.$$

As it can be seen, these expressions (13) are useful for the computation of references for high-speed operation vector control. The relative error is not exceeding (12).

Simulation results

The simulation of dynamics behavior of the traction drive system is needed for testing the proposed control structure. The simulation results are realized for the vector-controlled induction motor 180 KW, 1500 rpm in traction drive with speed sensor (Fig. 2) and speed sensorless (Fig. 3) in high-speed operating range including field weakening region.

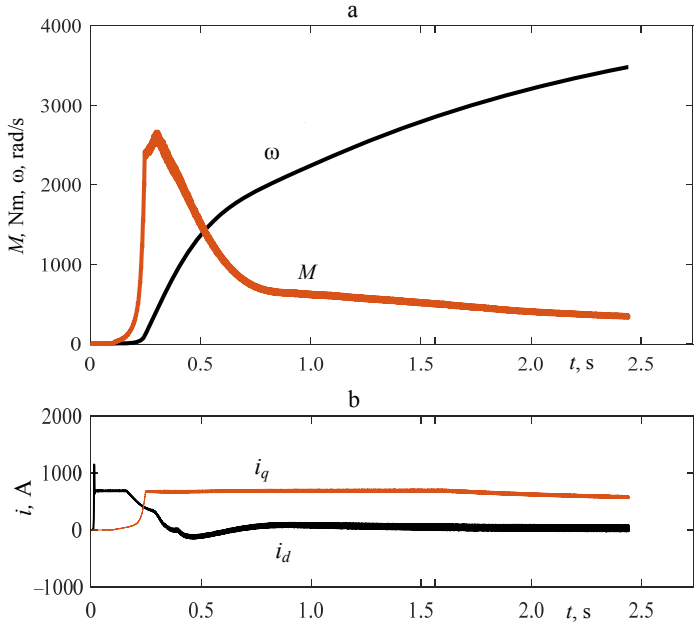

Fig. 2. Starting and speed acceleration with field weakening:
a – torque *M* and speed ω; b – current components i_d, i_q

Figure 2 shows the start and acceleration process with field weakening for the vector control system with speed sensor. There are three zone of the operation [5, 6] when field weakening is in usage. The first one is from zero to the nominal speed, that is seen in Fig. 2 for the time t <0.5 s. In the second zone the field is weakening with the maximal stator current in the time interval from $t \approx 0.5$ s to $t \approx 1.6$ *s*. In the third zone, $t > 1.6$ s the flux weakening control provides the maximal voltage with i_d decreasing so, that $i_d/i_q = \omega_s/\alpha = \text{const}$.

In the Fig. 3 the start and acceleration process with field weakening for the speed sensorless vector control is shown. The sensorless system is more critical for the internal and external disturbances and, as it is shown in Fig. 3a, has the ripples in torque in accelerating. In addition, with the sensorless control, the dynamics of the system becomes slower. Hence, the speed increases less intensive in Fig. 3, then for the system with speed sensor in Fig. 1.

From the comparison of Fig. 2, 3, the torque and acceleration are lover in case of Fig. 3. However, in both cases the dynamics performance is appropriate for the traction applications.

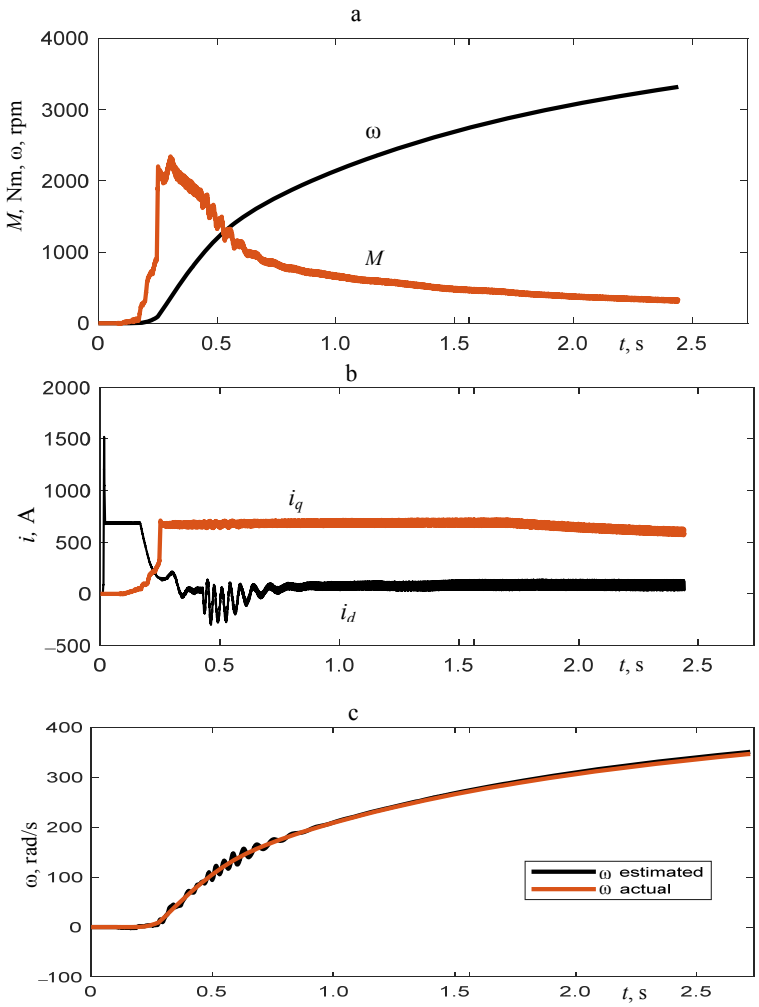

Fig. 3. Speed sensorless system, starting and speed acceleration with field weakening: a – torque M and speed ω; b – current components i_d, i_q; c – estimated and actual speed

CONCLUSIONS

1. The expressions (14) can be useful for references flux Ψ^* and torque current i_q^* real time computation. Such expressions provide correct operating of the system via the cost criteria, avoiding regulators saturation. The expressions (14) are approximate, then the absolute and relative errors are estimated through (11)–(13).

2. The simulations results demonstrate the efficiency of the real time implementation of the expressions (8), (10) in vector control system in high-speed operating range including field weaking region for the torque control in the system with speed sensor and in speed sensorless system.

REFERENCES

1. Blaschke F. (1972) Das Verfahren der Feldorientierung zur Regelung der Asynchronmaschine. *Siemens-Forsch und Entwicklungsber,* (1), 184–193 (in German).
2. Firago B. I., Vasiliev D. S. (2016) *Vector Control Systems for Electric Drive*. Minsk, Vysheishaya Shkola Publ. 159 (in Russian).
3 Opeiko O. F., Ptashnik A. I., Khilmon V. I. (2010) Tractional Electric Drive with Non-Sensing Element Vector Control System. *Energetika. Izvestiya Vysshikh Uchebnykh Zavedenii i Energeticheskikh Ob'edinenii SNG = Energetika. Proceedings of CIS Higher Education Institutions and Power Engineering Associations,* (6), 37–43 (in Russian).
4. Opeiko O. F. (2022) Synthesis Based on Linearization of Vector Speed Control of an Induction Motor without a Speed Sensor. *Energetika. Izvestiya Vysshikh Uchebnykh Zavedenii i Energeticheskikh Ob'edinenii SNG = Energetika. Proceedings of CIS Higher Education Institutions and Power Engineering Associations,* 65 (2), 103–114 (in Russian). https://doi.org/10.21122/1029-7448-2022-65-2-103-114.
5. Xu X., Novotny D. W. (1992) Selection of the Flux Reference for Induction Machine Drives in the Field Weakening Region. *IEEE Transactions on Industry Applications*, 28 (6), 1353–1358. https://doi.org/10.1109/28.175288.
6. Kim S. H., Sul S. K. (1995) Maximum Torque Control of an Induction Machine in the Field Weakening Region. *IEEE Transactions on Industry Application*s, 31 (4), 787–794. https://doi.org/10.1109/28.395288.
7. Gallegos-López G., Gunawan F. S., Walters J. E. (2007) Current Control of Induction Machines in the Field-Weakened Region. *IEEE Transactions on Industry Applications*, 43 (4), 981–989. https://doi.org/10.1109/TIA.2007.900459.
8. Mengoni M., Zarri L., Tani A., Serra G, Casadei D. (2008) Stator Flux Vector Control of Induction Motor Drive in the Field Weakening Region. *IEEE Transactions on Power Electronics*, 23 (2), 941–948. https://doi.org/10.1109/TPEL.2007.915636.
9. Lin P.-Y., Lai Y.-S. (2011) Novel Voltage Trajectory Control for Field-Weakening Operation of Induction Motor Drives. *IEEE Transactions on Industry Applications,* 47 (1), 112–127. https://doi.org/10.1109/TIA.2010.2091092.
10. Kim S. H., Sul S. K. (1997) Voltage Control Strategy for Maximum Torque Operation of an Induction Machine in the Field-Weakening Region. *IEEE Transactions on Industrial Electronics*, 44 (4), 512–518. https://doi.org/10.1109/41.605628.
11. Casadei D., Mengoni M., Serra G., Tani A., Zarri L. (2010) A Control Scheme with Energy Saving and DC-Link Overvoltage Rejection for Induction Motor Drives of Electric Vehicles. *IEEE Transactions on Industry Applications,* 46 (4), 1436–1446. https://doi.org/10.1109/TIA.2010.2049627.
12. Mengoni M., Zarri L., Tani A., Serra G., Casadei D. (2012) A Comparison of Four Robust Control Schemes for Field-Weakening Operation of Induction Motors. *IEEE Transactions on Power Electronics,* 27 (1), 307–320. https://doi.org/10.1109/TPEL.2011.2156810.
13. Seok J.-K., Kim S. H. (2015) Hexagon Voltage Manipulating Control (HVMC) for AC Motor Drives Operating at Voltage Limit. *IEEE Transactions on Industry Applications,* 51 (5), 3829–3837. https://doi.org/10.1109/TIA.2015.2416125.
14. Sahoo S. K., Bhattacharya T. (2016) Field Weakening Strategy for a Vector-Controlled Induction Motor Drive Near the Six-Step Mode of Operation. *IEEE Transactions on Power Electronics,* 31 (4), 3043–3051. https://doi.org/10.1109/TPEL.2015.2451694.

15. Su J., Gao R., Husain I. (2018) Model Predictive Control Based Field-Weakening Strategy for Traction EV Used Induction Motor. *IEEE Transactions on Industry Applications,* 54 (3), 2295–2304. https://doi.org/10.1109/TIA.2017.2787994.
16. Dong Z., Yu Y., Li W., Wang B., Xu D. (2018) Flux-Weakening Control for Induction Motor in Voltage Extension Region: Torque Analysis and Dynamic Performance Improvement. *IEEE Transactions on Industrial Electronics,* 65 (5), 3740–3751. https://doi.org/10.1109/TIE.2017.2764853.
17. Xu Y., Morito C. Lorenz R. D. (2019) Extending High-Speed Operating Range of Induction Machine Drives Using Deadbeat-Direct Torque and Flux Control with Precise Flux Weakening. *IEEE Transactions on Industry Applications,* 55 (4), 3770–3780. https://doi.org/10.1109/TIA.2019.2908342.
18. Wang B., Zhang X., Yu Y., Zhang J., Xu D. B. (2019) Maximum Torque Analysis and Extension in Six-Step Mode-Combined Field-Weakening Control for Induction Motor Drives. *IEEE Transactions on Industrial Electronics,* 66 (12), 9129–9138. https://doi.org/10.1109/TIE.2018.2889622.
19. Dong Z., Wang B., Yu Y., Zhang X., Zhang J., Xu D., Ding Z. (2019) Operating Point Selected Flux-Weakening Control of Induction Motor for Torque-Improved High-Speed Operation Under Multiple Working Conditions. *IEEE Transactions on Power Electronics,* 34 (12), 12011–12023. https://doi.org/10.1109/TPEL.2019.2905536.
20. Peng Z. (2020) Analysis and Implementation of Constrained MTPA Criterion for Induction Machine Drives. *IEEE Access,* 8, 176445–176453. https://doi.org/10.1109/ACCESS.2020.3024195.
21. Zhang X., Wang B., Yu Y, Zhang J., Dong J., Xu D., (2020) Analysis and Optimization of Current Dynamic Control in Induction Motor Field-Weakening Region. *IEEE Transactions on Power Electronics,* 35 (9), 8860–8866. https://doi.org/10.1109/TPEL.2020.2968978.
22. Tarvirdilu-Asl R., Nalakath S., Xia Z., Sun Y, Wiseman J., Emadi A. (2020) Improved Online Optimization-Based Optimal Tracking Control Method for Induction Motor Drives. *IEEE Transactions on Power Electronics,* 35 (10), 10654–10672. https://doi.org/10.1109/TPEL.2020.2976037.
23. Zhang X. Wang B., Yu Y, Zhang J., Dong J., Xu D. (2021) Circular Arc Voltage Trajectory Method for Smooth Transition in Induction Motor Field-Weakening Control. *IEEE Transactions on Industrial Electronics,* 68 (5), 3693–3706. https://doi.org/10.1109/TIE.2020.2988190.
24. Harikrishnan P., Hatua K., Rao S. E. (2022) A Quick Dynamic Torque Control for an Induction-Machine-Based Traction Drive During Square-Wave Mode of Operation. *IEEE Transactions on Industrial Electronics,* 69 (7), 6519–6529. https://doi.org/10.1109/TIE.2021.3095805.
25. Dordea T., Hoancă V., Păun Ş. Biriescu M., Madescu G., Liuba G., Moţ M. (2011) Direct-Drive Induction Motor for Railway Traction Applications. *Proceedings of the Romanian Academy, Series A,* 12 (3), 239–248.
26. Popescu M., A. Bitoleanu A., Dobriceanu M., Goreci L. (2019) Optimal Control Method of an Asynchronous Traction Motor. *11th International Symposium on Advanced Topics in Electrical Engineering,* March 28–30, 2019 Bucharest, Romania. https://doi.org/10.1109/ATEE. 2019.8724969.
27. Zhao N., Schofield N. (2020) An Induction Machine Design With Parameter Optimization for a 120 kW Electric Vehicle. *IEEE Transactions on Transportation Electrification,* 6 (2), 592–601. https://doi.org/10.1109/TTE.2020.2993456.
28. Xie F., Hong W., Wu W., Liang K., Qiu C. (2019) Current Distribution Method of Induction Motor for Electric Vehicle in Whole Speed Range Based on Gaussian Process. *IEEE Access,* 7 (13), 165974–165984. https://doi.org/10.1109/ACCESS.2019.2953293.
29. Brandstetter P., Kuchar M. (2017) Sensorless Control of Variable Speed Induction Motor Drive Using RBF Neural Network. *Journal of Applied Logic,* 24 (Part A), 97–108. https://doi.org/10.1016/j.jal.2016.11.017.
30. Odnolko D. S. (2013) Algorithm for Identification Electromagnetic Parameters of an Induction Motor When Running on a Three-Phase Power Plant. *Energetika. Izvestiya Vysshikh Uchebnykh Zavedenii i Energeticheskikh Ob'edinenii SNG = Energetika. Proceedings of CIS Higher Education Institutions and Power Engineering Associations,* (1), 47–55 (in Russian).
31. Adnolka D. (2013) Algorithm for Parametric Identification of Induction Motors and Its Experimental Testing. *Visnik Kremenchuts'kogo natsional'nogo universitetu imeni Mikhaila Ostrograds'kogo = Transactions of Kremenchuk Mykhailo Ostrohradskyi National University,* (4), 9–14 (in Russian).
32. Tytiuk V. K., Baranovskaya M. L., Chornyi O. P., Burdilnaya E. V., Kuznetsov V. V., Bogatyriov K. N. (2020) Online-Identification of Electromagnetic Parameters of an Induction Motor. *Energetika. Izvestiya Vysshikh Uchebnykh Zavedenii i Energeticheskikh Ob'edinenii SNG = Energetika. Proceedings of CIS Higher Education Institutions and Power Engineering Associations,* 63 (5), 423–440. https://doi.org/10.21122/1029-7448-2020-63-5-423-440.

Received: 21 October 2022 Accepted: 27 December 2022 Published online: 31 May 2023